Available online at www.sciencedirect.com
ScienceDirect
Journal of Solid State Chemistry 181 (2008) 884–894
JOURNAL OF SOLID STATE CHEMISTRY
www.elsevier.com/locate/jssc

Hydrothermal synthesis, crystal structure, thermal behavior and spectroscopic and magnetic properties of two new organically templated fluoro-vanadyl-hydrogenarsenates: $(R)_{0.5}[(VO)(HAsO_4)F]$ (R: Ethylenediammonium and piperazinium)

Teresa Berrocal[a], José L. Mesa[b,*], José L. Pizarro[a], Luis Lezama[b], Begoña Bazán[a], María I. Arriortua[a], Teófilo Rojo[b]

[a]*Departamento de Mineralogía y Petrología, Facultad de Ciencia y Tecnología, Universidad del País Vasco/EHU Apdo. 644, E-48080 Bilbao, Spain*
[b]*Departamento de Química Inorgánica, Facultad de Ciencia y Tecnología, Universidad del País Vasco/EHU Apdo. 644, E-48080 Bilbao, Spain*

Received 19 November 2007; received in revised form 22 January 2008; accepted 26 January 2008
Available online 6 February 2008

Abstract

Two new fluoro-vanadyl-hydrogenarsenate compounds templated by ethylenediamine and piperazine with formula, $(C_2N_2H_{10})_{0.5}[(VO)(HAsO_4)F]$ **(1)** and $(C_4N_2H_{12})_{0.5}[(VO)(HAsO_4)F]$ **(2)**, respectively, have been synthesized by using mild hydrothermal conditions under autogenous pressure. The crystal structures have been solved from single-crystal X-ray diffraction data. The phases crystallize in the $P2_1/c$ monoclinic space group with the unit-cell parameters $a = 7.8634(4)$ Å, $b = 7.7658(4)$ Å, $c = 10.4195(6)$ Å, $\beta = 101.524(5)^\circ$ for compound **(1)** and $a = 6.301(1)$ Å, $b = 10.244(1)$ Å, $c = 10.248(1)$ Å and $\beta = 95.225(1)^\circ$ for compound **(2)**. These phases exhibit a layered inorganic framework. In both cases, the structure is built from secondary building units (SBU) which are formed by $[V_2O_8F_2]$ edge-shared dimeric vanadyl octahedra, connected by the vertices to two hydrogenarsenate tetrahedra. The repetition of this SBU unit originates sheets along the [1 0 0] direction. The ethylenediammonium and piperazinium cations are located inside the interlayer space. The limit of thermal stability for compounds **(1)** and **(2)** is, approximately, 250 and 230 °C, respectively. Near this temperature, both phases loose their organic cations and the fluoride anions. The diffuse reflectance spectra confirm the presence of vanadyl ions, in which the vanadium(IV) cations have a d^1 electronic configuration in a slightly distorted octahedral environment. ESR spectra of both phases are isotropic with mean g-values of 1.93 and 1.96 for ethylendiamine and piperazine phases, respectively. Magnetic measurements for **(1)** and **(2)** indicate the existence of antiferromagnetic exchange couplings.

Keywords: Hydrothermal synthesis; Vanadyl arsenates; Crystal structure; ESR; Magnetism

1. Introduction

The design and synthesis of organically templated hybrid materials have been of great interest due to their unusual topological properties and potential applications in the fields of catalysis, biochemistry, magnetism and material science [1–3].

In the area of open-framework structures, the phosphate compounds are the predominant class [1]. Although arsenic belongs to the same group of the Periodic Table as phosphorous, little work has been carried out on arsenates organically templated. In this sense, the research about this kind of compounds is now emerging. We have recently studied the formation of novel iron arsenates employing the hydrothermal synthesis in presence of structure-directing amine molecules [4]. It is manifested that the structure variety of vanadium compounds is plenty, since the oxidation state of vanadium may vary among +3, +4 and +5, and its polyhedra can be tetrahedral, square pyramid, trigonal bipyramid and octahedron [5]. The flexibility of coordination and the variation in oxidation states are beneficial to some practical applications, as such as, coordination intercalation and catalyst [6,7].

*Corresponding author. Fax: +34 946013500.
E-mail address: joseluis.mesa@ehu.es (J.L. Mesa).

0022-4596/$ - see front matter © 2008 Elsevier Inc. All rights reserved.
doi:10.1016/j.jssc.2008.01.037

According to the results of our literature research, some organically templated vanadyl arsenates have been reported, all of which exhibit chain structure [8,9]. The butanediammonium, $(H_2NC_4H_8NH_2)[(VO)_2(HAsO_4)_2(H_2AsO_4)_2]$ phase contains –V=O–V=O– chains [8]. The two ethylenediammonium, $(H_3C_2H_4NH_3)[(VO)(As_2O_7)(H_2O)]$ and $(H_3C_2H_4NH_3)_{0.5}[(VO)(AsO_4)(H_2O)]$, compounds exhibit isolated chains [9]. The finite organic chains run parallel to the –V–O–As_2–O–V– chains in the diarsenate whereas they are orthogonal to the $-V_2-O-As-O-V_2-$ chains in the monoarsenate. Similarly, some vanadyl phosphates templated with diamines have been synthesized [10–14]. The crystal structure of $(H_3C_2H_4NH_3)[(VO)_3(PO_4)_2(HPO_4)(H_2O)_2]$ consists of binuclear units of $[VO_6]$ corner-shared octahedra and $[VO_5]$ square pyramids, linked by phosphate tetrahedra, forming double extended polyhedral slabs in the (101) plane, with these slabs connected by $[HPO_4]$ corner-shared tetrahedra to form a three-dimensional structure about the diammonium cations [10]. Both, the $(H_2NC_4H_8NH_2)[(VO)_2(PO_4)_2]$ and $(H_2NC_4H_8NH_2)_2[(VO)_3(HPO_4)_2(PO_4)_2]\cdot H_2O$ phases, have a layered structure which contain corner-shared (VO_5) triangular bipyramidal and (VO_6) octahedral vanadium(IV) centers together with (VO_5) square pyramids, respectively [11]. The four two-dimensional vanadyl phosphates with formula, $(H_3dien)[(VOPO_4)(OH)]\cdot(H_2O)$ (dien = diethylentriamine), $(H_2dach)_{1.5}[(VOPO_4)_2(OH)]\cdot(H_2O)$ (dach = 1,4-diaminocyclo hexano), $(H_2tmdpp)[V_3O_4(OH)(PO_4)_2]\cdot 3H_2O$ (tmdpp = 4,4′-trimethylenedipiperazine) and $(H_2tmdpp)[V_5O_7(H_2O)_2(PO_4)]\cdot(H_2O)$, exhibit layered topologies with ($V^{IV}O_5$) square pyramids, (PO_4) tetrahedra and discrete dimers of V–O polyhedra [12]. The mixed valence piperazine-vanadium phosphates $(C_4H_{12}N_2)(H_3O)[(VOPO_4)_4(H_2O)(H_2PO_4)]\cdot 3H_2O$ and $(C_4H_{12}N_2)[(VO)(VO_2)(H_2O)(PO_4)_2]$ also exhibit layered structures. In the first one, the $[(VOPO_4)_4(H_2O)(H_2PO_4)]^{3-}$ framework is constructed by connecting $(VOPO_4)_4(H_2O)$ layers through bridging tetrahedral $PO_2(OH)_2$ groups. In the second one, the

Table 1
Crystal data, details of data collection, and structure refinement for $(C_2N_2H_{10})_{0.5}[(VO)(HAsO_4)F]$ and $(C_4N_2H_{12})_{0.5}[(VO)(HAsO_4)F]$

Empirical formula	CNH_6VOAsO_5F	$C_2NH_7VOAsO_5F$
Formula weight ($g\,mol^{-1}$)	256.93	269.95
Crystal system	Monoclinic	Monoclinic
Space group (no. 33)	$P2_1/c$	$P2_1/c$
a (Å)	7.8634(4)	6.301(1)
b (Å)	7.7658(4)	10.244(1)
c (Å)	10.4195(6)	10.248(1)
β (°)	101.524(5)	95.225(1)
V (Å^3)	623.45(6)	658.7(1)
Z	4	4
ρ_{obs}, ρ_{calc} ($g\,cm^{-3}$)	2.69(2), 2.73	2.70(1), 2.72
$F(0\,0\,0)$	496	524
μ (mm^{-1})	6.845	6.486
Radiation, λ (Mo$K\alpha$) (Å)	0.71073	0.71073
Collected reflections	2927	4106
Independent reflections	1062	1202
Interval h, k, l	$-8<h\leqslant 9$, $k\pm 9$, $l\pm 11$	$h\pm 7$, $k\pm 12$, $l\pm 12$
R(int)	0.0340	0.0271
$R[I>2\sigma(I)]$	$R_1=0.0301$, $wR_2=0.0698$	$R_1=0.0197$, $wR_2=0.0449$
R[all data]	$R_1=0.0432$, $wR_2=0.0720$	$R_1=0.0265$, $wR_2=0.0468$
$\Delta_{\rho max}$ and $\Delta_{\rho min}$ ($e\,Å^{-3}$)	0.605, −0.488	0.356, −0.533
G.O.F.	0.942	0.950

$R_1=[\Sigma(|Fo|-|Fc|)]/\Sigma|Fo|$; $wR_2=\Sigma(w|Fo|^2-|Fc|^2)^2]/\Sigma[w(|Fo|^2)^2]^{1/2}$, $w=1/[\sigma^2|Fo|^2+(0.0410p)^2]$, where $p=(|Fo|^2+2|Fc|^2)/3$.

Table 2
Fractional atomic coordinates and equivalent isotropic displacement parameters ($\times 10^3$ Å^2) for $(C_2N_2H_{10})_{0.5}[(VO)(HAsO_4)F]$

Atoms	x	y	z	U(eq)
V	0.3272(1)	0.0885(1)	−0.0965(1)	7(1)
As	0.3449(1)	0.0609(1)	0.2126(1)	11(1)
O(1)	0.2800(4)	0.1734(4)	0.0754(2)	11(1)
O(2)	0.5433(4)	−0.0247(4)	0.2353(3)	12(1)
O(3)	0.3249(4)	0.1696(4)	0.3487(3)	13(1)
O(4)	0.1346(4)	0.0296(4)	−0.1695(3)	17(1)
O(5)	0.2087(4)	−0.1138(4)	0.2113(4)	19(1)
N(1)	−0.2332(5)	0.0680(5)	0.4708(4)	12(1)
C(1)	−0.0432(6)	0.0856(5)	0.4959(5)	14(1)
F	0.5954(3)	0.1295(3)	0.0075(2)	10(1)
H(1)	0.1090	−0.0800	0.2073	68(6)
H(2)	−0.2755	0.1299	0.5292	68(6)
H(3)	−0.2611	−0.0423	0.4776	68(6)
H(4)	−0.2780	0.1056	0.3905	68(6)
H(5)	−0.0044	0.1474	0.5773	68(6)
H(6)	−0.0101	0.1521	0.4254	68(6)

Table 3
Fractional atomic coordinates and equivalent isotropic displacement parameters ($\times 10^3$ Å^2) for $(C_4N_2H_{12})_{0.5}[(VO)(HAsO_4)F]$

Atoms	x	y	z	U(eq)
V	0.6045(1)	0.1215(1)	−0.0813(1)	6(1)
As	0.3877(1)	0.1729(1)	0.1861(1)	7(1)
O(1)	0.5557(3)	0.2247(2)	0.0812(2)	11(1)
O(2)	0.4133(3)	0.0131(2)	0.2261(2)	9(1)
O(3)	0.3993(3)	0.2607(2)	0.3213(2)	15(1)
O(4)	0.8304(3)	0.1821(2)	−0.1072(2)	18(1)
O(5)	0.1261(3)	0.1992(2)	0.1212(3)	17(1)
N(1)	−0.1214(4)	0.0620(2)	0.5957(3)	12(1)
C(1)	0.2249(5)	−0.0117(3)	0.5311(3)	14(1)
C(2)	0.0765(6)	−0.0127(3)	0.6370(3)	16(1)
F(1)	0.6918(3)	−0.0249(2)	0.0345(2)	10(1)
H(1)	0.1100(60)	0.1550(30)	0.0470(20)	21(4)
H(2)	0.3380(40)	−0.0660(30)	0.5480(40)	21(4)
H(3)	0.1470(50)	0.0200(30)	0.7100(30)	21(4)
H(4)	0.0410(50)	−0.0940(20)	0.6530(40)	21(4)
H(5)	−0.0990(60)	0.1466(19)	0.5910(40)	21(4)
H(6)	−0.2200(40)	0.0550(30)	0.6520(30)	21(4)
H(7)	0.2660(50)	0.0720(20)	0.5100(30)	21(4)

$[(VO)(VO_2)(H_2O)(PO_4)_2]^{2-}$ sheets, separated by diprotonated piperazine cations, contain $V^{IV}O_6$ distorted octahedra, two $V^{V}O_5$ trigonal bipyramids and two PO_4 tetrahedra, connecting by sharing oxygen atoms [13]. Finally, the ethylenediammonium mixed-valent vanadyl phosphate, $(H_3NC_2H_4NH_3)_{0.5}[V^{4+}_{0.45}V^{5+}_{0.55}O_2PO_4\{P(OH)_2\}_{0.483}]$ also has a layered structure [14]. It is remarkable the absence of fluoride anions in the composition of these organically templated vanadyl arsenates and phosphates. The incorporation of this anion in the inorganic framework of the title compounds, following the synthetic route opened by Keller and co-workers [15], it makes possible the synthesis of original and not structurally related phases with those ones found in the literature.

During the course of our study in order to obtain new organically templated vanadium–arsenate phases, we have synthesized two new fluoro-vanadyl-hydrohenarsenates with the ethylenediamine and piperazine as templating agents. These compounds have the formula $(R)_{0.5}[(VO)(HAsO_4)F]$. In this work, we report on their crystal structure, thermal behavior, spectroscopic, and ESR and magnetic susceptibility.

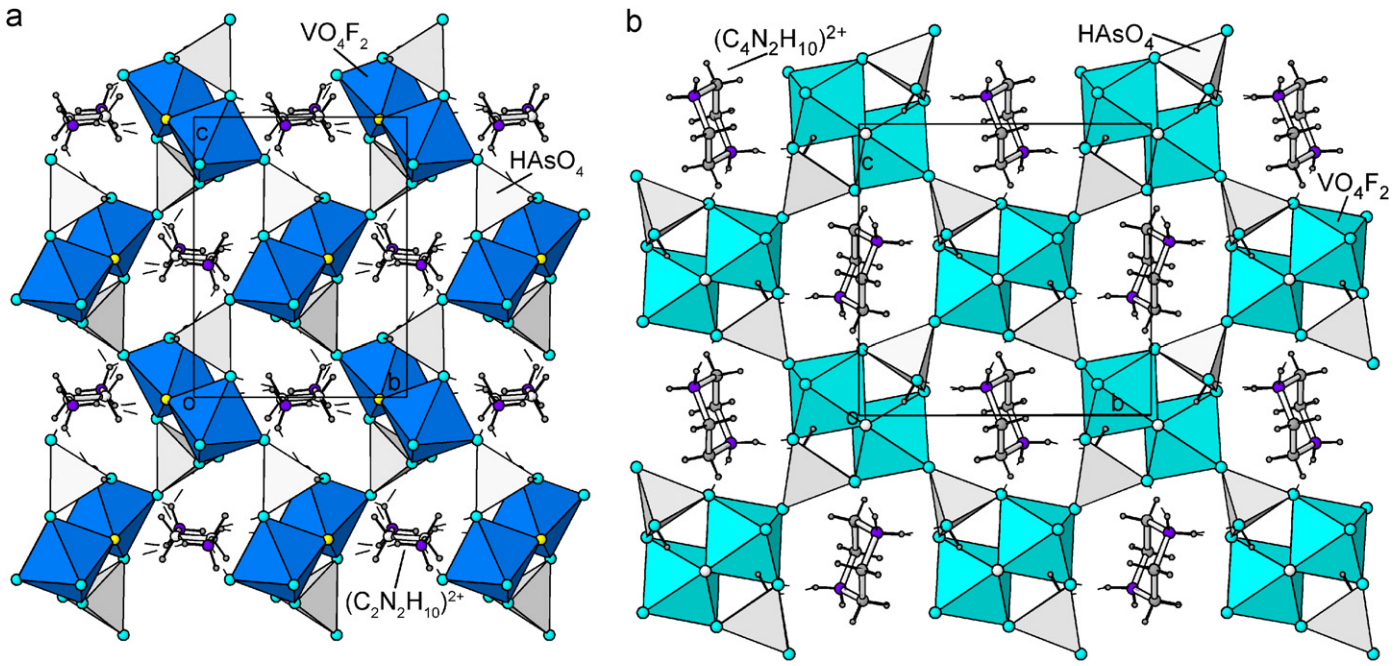

Fig. 1. Polyhedral view of the sheets for (a) compounds **(1)** and (b) **(2)**.

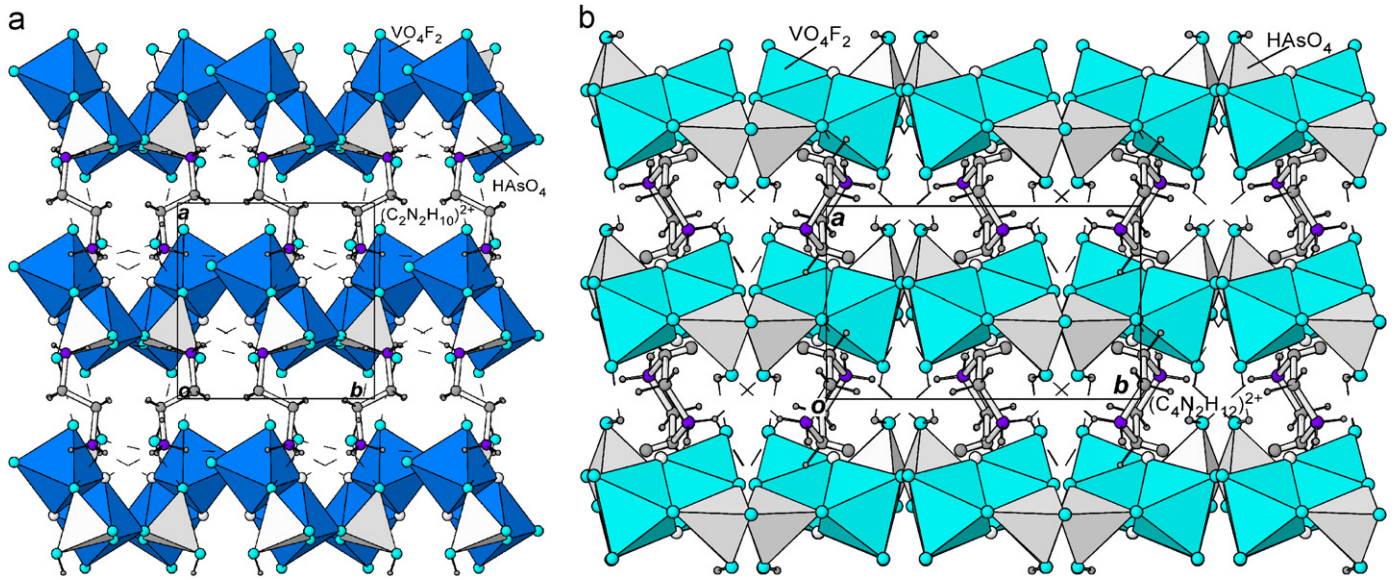

Fig. 2. Polyhedral view of the layered crystal structure for (a) compounds **(1)** and (b) **(2)**.

2. Experimental

2.1. Hydrothermal synthesis and chemical characterization

Phases **(1)** and **(2)** were synthesized by using mild hydrothermal conditions under autogenous pressure. The reagents, V_2O_3 (2.335 and 2.001 mmol for **(1)** and **(2)**, respectively) and $As_2O_5 \cdot 3H_2O$ (3.690 mmol in both cases) were solved in a mixture of 20 mL of water and 10 mL ethanol for **(1)** and 30 mL of water for **(2)**, then 1 mL of HF (57.5 mmol) was added in each case. Finally, the ethylenediamine and pyperazine molecules were used in order to fix the pH at, approximately, 3 and 1, respectively. These reaction mixtures were stirred to assure homogeneity, sealed in a PTFE-lined stainless steel pressure vessel (filling factor 75%) and then heated at 170 °C for 5 days. After reaction, slow cooling, at 30 K per hour, until room temperature was carried out. The pH did not show any appreciable change during the hydrothermal treatment. The compounds were obtained as prismatic light and intense green single crystals, for **(1)** and **(2)**, respectively. The size of the crystals is $0.1 \times 0.08 \times 0.04\,mm^3$ for **(1)** and $0.01 \times 0.03 \times 0.01\,mm^3$ for **(2)**. The yield was, approximately, 80% in both cases.

The chemical composition of the two compounds was calculated by atomic absorption spectroscopy (A.A.S.) and C,H,N-elemental analysis. The amount of the fluoride anions was calculated by using a selective electrode. Compound **(1)** has the formula $(C_2N_2H_{10})_{0.5}[(VO)(HAsO_4)F]$. Calc: N, 5.4; H, 2.3; C, 4.7; As, 29.2; V, 19.8; F, 7.4. Found: N, 5.3; H, 2.2; C, 4.6; As, 29.1; V, 19.7; F, 7.3. The chemical formula for **(2)** is $(C_4N_2H_{12})_{0.5}[(VO)(HAsO_4)F]$. Calc: N, 5.2; H, 2.6; C, 8.9; As, 27.7; V, 18.9; F, 7.0. Found: N, 5.1; H, 2.5; C, 8.8; As, 27.5; V, 18.7; F, 6.9. The densities, measured in a mixture of bromoform (Br_3CH, $\rho = 2.82\,g\,cm^{-3}$) and chloroform (Cl_3CH, $\rho = 1.476\,g\,cm^{-3}$), are 2.69(2) and 2.70(1) $g\,cm^{-3}$, respectively.

2.2. Single-crystal X-ray diffraction experiments and structure solution

Single crystals of **(1)** and **(2)** were carefully selected under a polarizing microscope and mounted on a glass fibre. Single-crystal X-ray diffraction data were collected at room temperature on an Oxford Diffraction XCALIBUR2 automatic diffractometer equipped with a CCD detector for **(1)** and on a STOE IPDS (Imaging Plate Diffraction System) automatic diffractometer for **(2)**. The Mo$K\alpha$ radiation was used in both cases. The Lorentz-polarization and absorption corrections were made with the diffractometer software [16,17], taking into account the shape and size of the single crystals. The structures were solved by direct methods with the SHELXS97 computer program [18]. At the first, the positions of the vanadium(IV), arsenic(V) and the oxygen atoms were located. SHELXL97 [19] was used to refine the structure by the least-squares method based on F^2. The refinement procedure allowed to identify the rest of the oxygen and fluorine atoms. Scattering factors were taken from Ref. [20]. Anisotropic atomic displacement parameters were used to refine all the atoms, except the hydrogen ones. Details of crystal data, intensity collection and some features of the structural refinement are given in Table 1, together with the final *R*-factors. The X-ray powder diffraction patterns of both phases were in good agreement with those obtained from the single-crystal data. The final atomic coordinates and thermal parameters have been deposited at the Cambridge Crystallographic Data Centre (CCDC 668020 and 668019 for **(1)** and **(2)**, respectively). All structure drawings were made using the ATOMS program [21]. Crystallographic data, atomic coordinates and selected bond distances and angles are listed in Tables 1–5, respectively.

2.3. Physicochemical characterization techniques

The analytical measurements were carried out by using atomic absorption spectroscopy with a grafit camera Zeeman Perkin-Elmer 4110 ZL. Diffuse reflectance spectra were measured at room temperature on a Cary 5000 spectrophotometer in the spectral range 2000–210 nm range. A Bruker ESP 300 spectrometer, operating at X band, was used to record the ESR polycrystalline spectra between 4.2 and 300 K. The temperature was stabilized by an Oxford Instrument (ITC 4) regulator. The magnetic field was measured with a Bruker BNM 200 guassmeter and the frequency inside the cavity was determined using a Hewlett-Packard 5352B microwave frequency counter. Magnetic measurements on powdered samples were performed in the temperature range 2.0–300 K, using a Quantum Design MPMS-7 SQUID magnetometer. The applied magnetic field

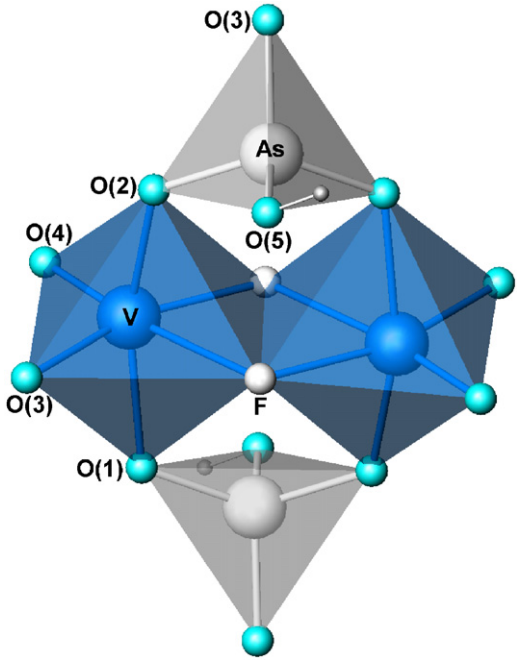

Fig. 3. SBU of the compounds **(1)** and **(2)**.

was 0.1 T, a value in the range of linear dependence of magnetization vs. magnetic field, even at 2.0 K.

3. Results and discussion

3.1. Crystal structure

$(R)_{0.5}[(VO)(HAsO_4)F]$, with R = ethylenediammonium and piperazinium, are layered compounds. The crystal structure consists in a two-dimensional inorganic skeleton, with composition $[(VO)(HAsO_4)F]^-$. The sheets are extended along the [1 0 0] direction (Fig. 1a and b). The ethylenediammonium and piperazinium cations are located in the interlayer space (Fig. 2a and b). These organic cations stabilize the crystal structure forming, both, ionic interactions and hydrogen bonds with the inorganic framework. The fluorine atoms establish interlayer hydrogen bonds of, approximately 2.7 Å, with the ethylenediammonium and piperazinium cations through the H(2) and H(1)-hydrogen atoms in compounds **(1)** and **(2)**,

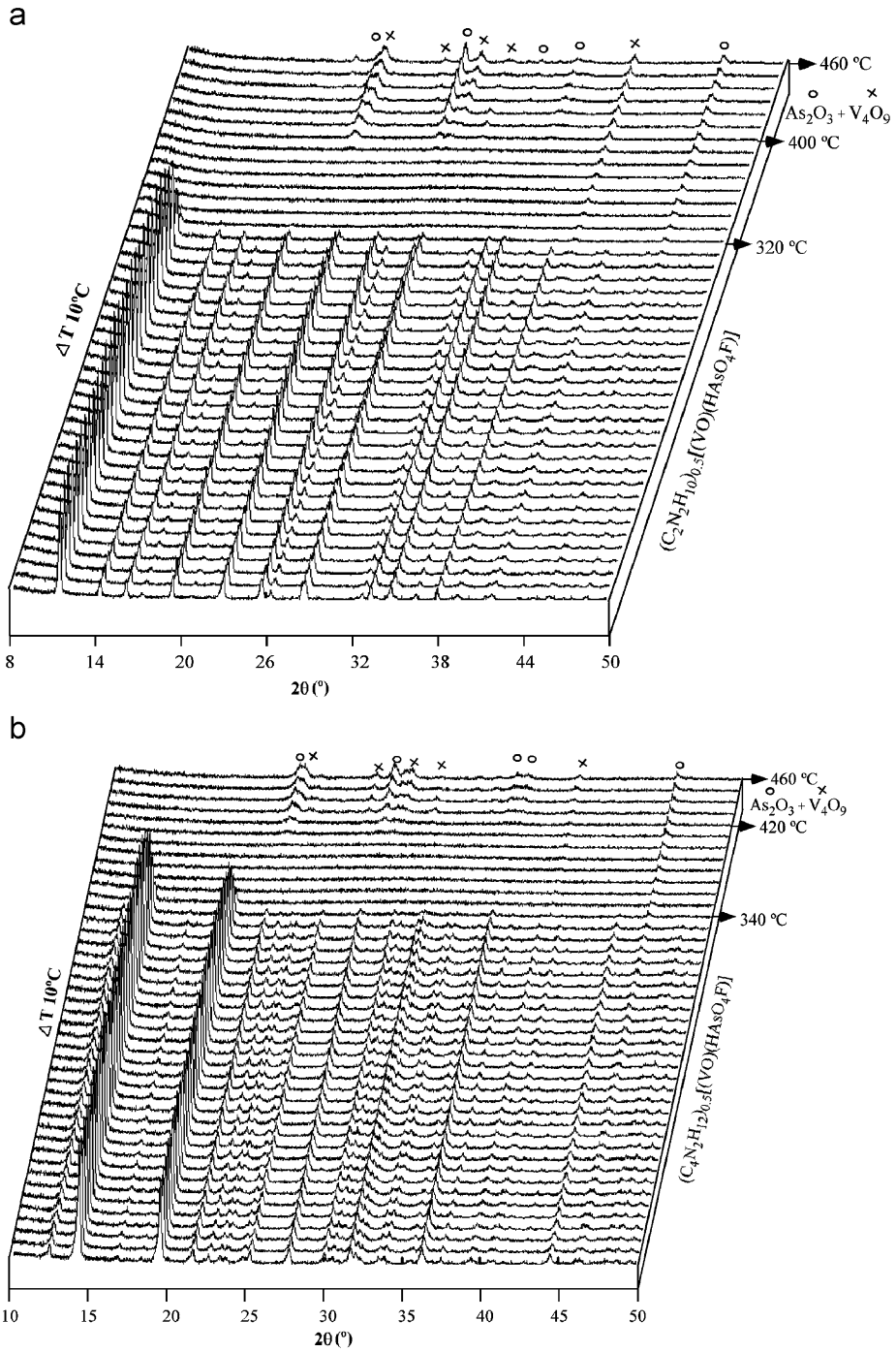

Fig. 4. Thermodiffractograms of the compounds (a) **(1)** and (b) **(2)**.

respectively. The rest of the hydrogen bonds, with a mean value of 2.9 Å, are established between the organic dications and the oxygen atoms of the hydrogenarsenate oxoanions, linking the sheets.

The $[(VO)(HAsO_4)F]^-$ layers are built from tetrameric SBU-4 units, formed by two F(1)–F(1)^i edge-shared $[V_2O_8F_2]$ dimer octahedra and two $[HAsO_4]$ tetrahedral groups. The dimers are connected, through the O(1), O(2) oxygen atoms, to two $[HAsO_4]$ tetrahedra (Fig. 3). The connection between the SBU-4 units takes place through the O(3) oxygen atoms. This SBU-4 unit has been found in the $(H_3C_2H_4NH_3)$ $[(VO)(As_2O_7)(H_2O)]$ phase [9] which exhibits a chain structure.

In the $[V_2O_8F_2]$ dimers, the O(4)-oxygen atoms that form the vanadyl cations exhibit a mean V = O bond distance of 1.60(1) Å, shorter than the rest of V–O bond distances, with a mean value of 1.98(3) Å. The O(1), O(2), O(3) and F(1)′ atoms occupy the *cis*-positions of the octahedra, whereas the F(1)-fluorine atoms occupy the *trans*-positions, together with the O(4) from the vanadyl cation.

In the $[VO_4F–F^i]$ octahedra, the V–O bond distances range from 1.611(3) to 2.011(3) Å for **(1)** and from 1.597(2) to 2.020(2) Å for **(2)**. The V–F bond lengths are in the 1.967(3)–2.193(3) and 1.960(1)–2.205(2) Å ranges, for **(1)** and **(2)**, respectively. The *cis*-(F,O)–V–(O,F) angles range from 73.5(1)° to 101.0(1)° for **(1)** and from 73.87(7)° to 103.3(1)° for **(2)**. Finally, the *trans*-(F,O)–V–(O,F) bond angles ranging between 160.1(1)–71.9(1)° and 155.51(9)–174.95(9)° for **(1)** and **(2)**, respectively.

Table 4
Selected bond distances (Å) and angles (°) for $(C_2N_2H_{10})_{0.5}[(VO)(HAsO_4)F]$

Octahedron $[VO_4F_2]$

V	O(1)	O(2)^{ii}	O(3)^i	O(4)	F	F^{ii}
F^{ii}	87.57(13)	88.47(12)	160.86(13)	98.70(15)	73.47(12)	1.967(3)
F	80.94(11)	79.28(11)	87.51(12)	171.93(15)	2.193(3)	
O(4)	100.96(16)	98.88(16)	100.38(16)	1.619(3)		
O(3)^i	87.28(13)	90.15(13)	1.963(3)			
O(2)^{ii}	160.14(14)	1.991(3)				
O(1)	2.011(3)					

Tetrahedron $[AsO_4]$

As	O(1)	O(2)	O(3)	O(5)
O(5)	108.83(17)	104.39(16)	103.78(16)	1.727(3)
O(3)	113.30(16)	108.79(16)	1.684(3)	
O(2)	116.61(16)	1.669(3)		
O(1)	1.666(3)			

Table 5
Selected bond distances (Å) and angles (°) for $(C_4N_2H_{12})_{0.5}[(VO)(HAsO_4)F]$

Octahedron $[VO_4F_2]$

V	O(1)	O(2)^{ii}	O(3)^{iv}	O(4)	F(1)	F(1)^{ii}
F(1)^{ii}	81.96(7)	82.08(7)	81.71(7)	174.98(9)	73.83(7)	2.2042(17)
F(1)	87.52(7)	85.21(7)	155.48(8)	101.15(9)	1.9593(15)	
O(4)	97.97(10)	97.67(10)	103.30(10)	1.598(2)		
O(3)^{iv}	87.42(8)	93.20(8)	1.9718(19)			
O(2)^{ii}	163.77(8)	2.0210(19)				
O(1)	2.020(2)					

Tetrahedron $[AsO_4]$

As	O(1)	O(2)	O(3)	O(5)
O(5)	109.89(10)	107.97(10)	101.78(10)	1.741(2)
O(3)	112.761(10)	109.18(10)	1.6482(19)	
O(2)	114.43(10)	1.6916(18)		
O(1)	1.663(2)			

The [$HAsO_4$] tetrahedra are linked to eight metallic cations through their three oxygen atoms O(1), O(2) and O(3). The O(5) atom is linked to a hydrogen one forming the O–H bonds, with interatomic bond distances of 0.82(1) Å for **(1)** and 0.89(1) Å for **(2)**. In these hydrogenarsenate groups, the mean value of the As–O bond distances is 1.687(1) and 1.686(3) Å, for **(1)** and **(2)**, respectively. The O–As–O angles range from 103.8(2)° to 116.6(1)° for **(1)** and from 101.8(1)° to 114.4(1)° for **(2)**, as expected for the tetrahedral geometry with a sp^3 hybridization on the arsenic atoms.

The distortion of the [VO_4F–F^i] octahedra from that of an ideal octahedron and trigonal prism was evaluated using the Alvarez et al.'s method [22]. The distortion is, approximately, $S(Oh) = 0.63$ and 0.66 for each polyhedron. In the [$HAsO_4$] tetrahedra, the distortion from an ideal tetrahedron is $S(Td) = 0.16$.

3.2. Thermal behavior

The thermogravimetric analysis of compounds **(1)** and **(2)** was carried out under synthetic air in a DSC 2960 simultaneous DSC-TGA instrument. Crucibles containing ca. 20 mg of each sample were heated at 5 °C min^{-1} in the temperature range 30–800 °C. The thermogravimetric curves show an exothermic mass loss of, approximately, 22% for both compounds, in the 250–340 and 230–340 °C ranges, for **(1)** and **(2)**, respectively. These mass losses can be attributed to the elimination of the fluoride anion and the organic cation (calc. 19.5% and 23.3%; exp. 22.0% and 23.0%, respectively). The proposed reaction for this step is: $(C_2N_2H_{10})[(VO)(HAsO_4)F]_2(s) + (9/2)O_2 \rightarrow F_2(g) + 2CO_2(g) + 5H_2O(g) + N_2(g) + 2(VO)(HAsO_4)(s)$. The second mass loss takes place in the 340–575 and 340–480 °C ranges for **(1)** and **(2)**, respectively. This later step corresponds to the decomposition of the hydrogenarsenate oxoanions and the formation of the inorganic residue, which was not possible identify by X-ray diffraction, because it remained linked to the crucible.

The thermal behavior of **(1)** and **(2)** was also studied by using time-resolved X-ray thermodiffractometry in air. A Bruker D8 Advance diffractometer (Cu$K\alpha$ radiation) equipped with, a variable-temperature stage (Paar Physica TCU2000), a Pt sample heater and a Vanter high-speed one-dimensional detector with three degrees of angular aperture, was used in the experiment. The power patterns were recorded in the range $8 \leqslant 2\theta \leqslant 50°$, collecting the diffractograms each 4 min, and increasing the temperature at 10 °C min^{-1} from room temperature to 460 °C (Fig. 4a and b). The results indicate that the phases are stable up to 320 and 340 °C for **(1)** and **(2)**, respectively. Above these temperatures, the diffraction peaks of the diffractograms lose intensity and finally disappear, with formation of an amorphous compound in the temperature ranges 320–400 °C for **(1)** and 340–420 °C for **(2)**. These facts indicate that the crystal structures collapse, as consequence of the calcination of the organic molecules and the elimination of the fluoride anions. Above 400 °C for **(1)** and 420 °C for **(2)** the inorganic residues are formed, which correspond in both phases to the V_4O_9(s) [*Pnma*, $a = 17.92$ Å, $b = 3.631$ Å, $c = 9.396$ Å] [23a] and As_2O_3(s) oxides [$P2_1/n$, $a = 7.990$ Å, $b = 4.650$ Å, $c = 9.120$ Å, $\beta = 78.30°$] [23b]. The proposed reaction for the formation of the inorganic residue is: $4(VO)(HAsO_4)(s) \rightarrow 2As_2O_3(s) + V_4O_9(s) + 2H_2O(g) + (3/2)O_2(g)$.

3.3. UV–vis spectroscopy

The diffuse reflectance spectra of the title compounds show three bands of frequencies ν_1: 11,555 and 11,800 cm^{-1}; ν_2: 14,905 and 15,635 cm^{-1} and ν_3: 21170 and 22170 cm^{-1} for **(1)** and **(2)**, respectively. If a C_{4v} ideal

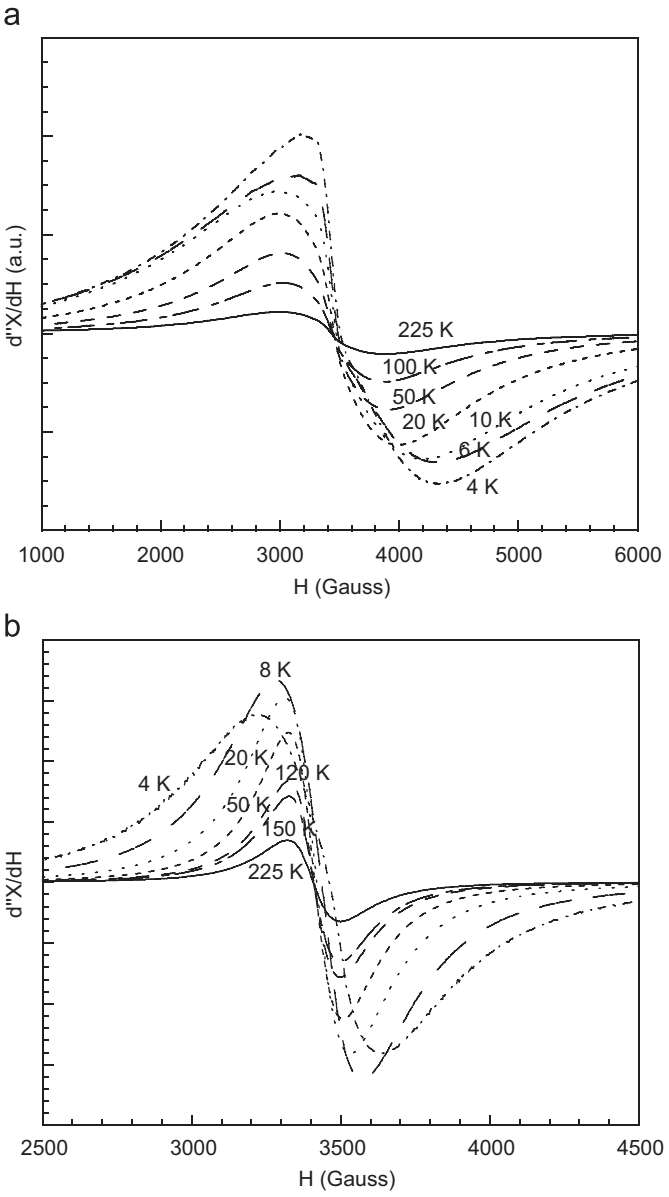

Fig. 5. X-band EPR spectra at selected temperatures for (a) compounds **(1)** and (b) **(2)**.

symmetry is supposed for the $[(VO)O_3F_2]$ chromophore, the assignment of the electronic transitions is ν_1: $^2B_2(xy) \rightarrow {}^2E(xz,yz)$, ν_2: $^2B_2(xy) \rightarrow {}^2B_1(x^2-y^2)$ and ν_3: $^2B_2(xy) \rightarrow {}^2A_1(z^2)$ [24]. Furthermore, a band due to a charge transference process, at a frequency near to 27,600 cm^{-1}, is observed in both spectra.

3.4. Magnetic behavior

3.4.1. ESR measurements

ESR spectra of the compounds **(1)** and **(2)**, recorded on powdered samples at X-band between 4.2 and 300 K, are given in Fig. 5. The spectra of both phases show isotropic

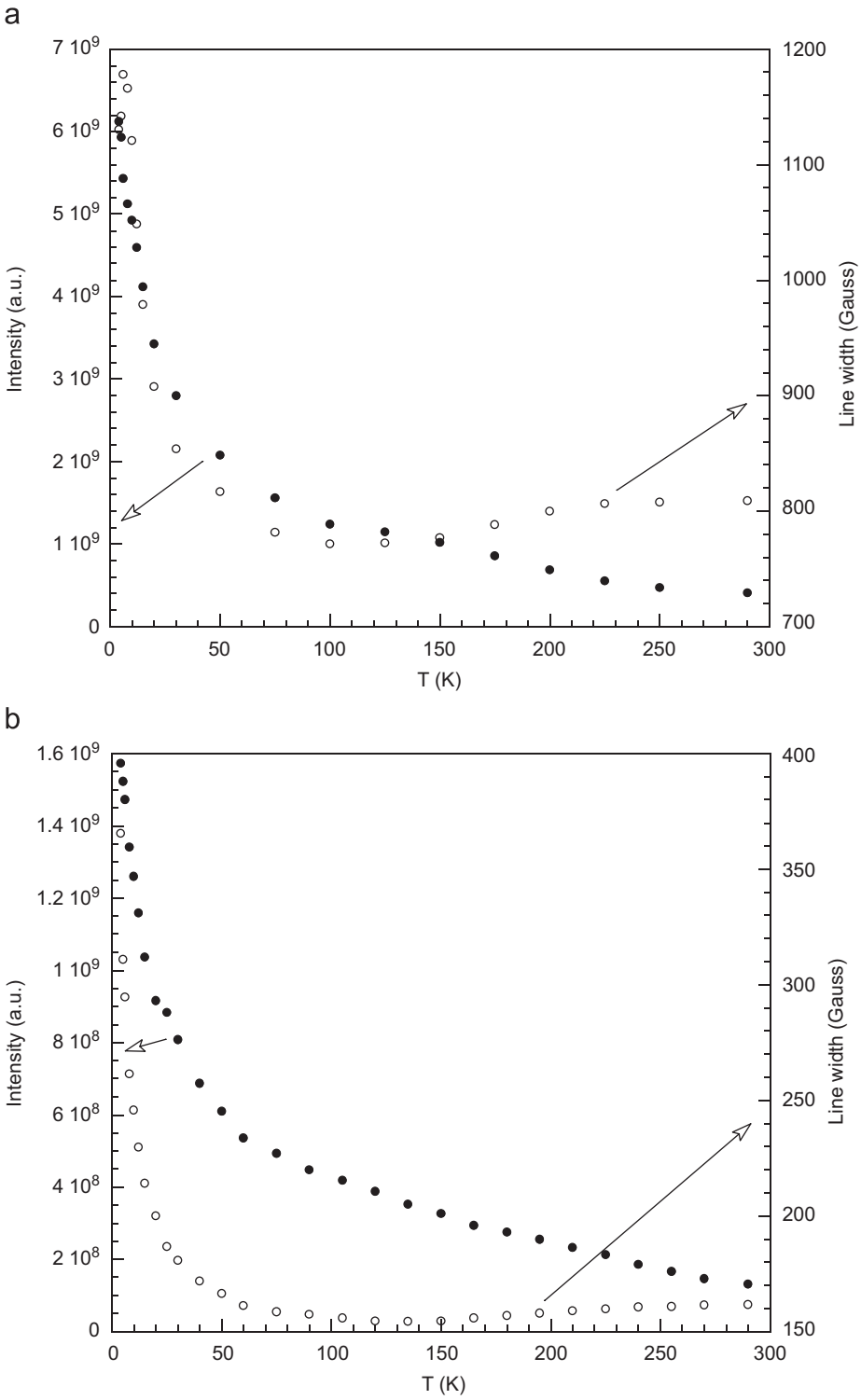

Fig. 6. Thermal evolution on the intensity and line width of the ESR signals for (a) compounds **(1)** and (b) **(2)**.

signals with a mean g-value of 1.93 and 1.96, for **(1)** and **(2)**, respectively. These values are characteristic of octahedrically coordinated $(VO)^{2+}$ vanadyl cations [25]. The temperature dependence of the intensity and the line width of the signals, calculated by fitting the experimental spectra to Lorentzian curves are shown in Fig. 6. The intensity of the signal increases in all the temperature ranges studied for both compounds. This behavior could be explained considering the compounds as either paramagnetic or antiferromagnetic systems, in which the maximum in the magnetic susceptibility is near 4.2 K, the minimum temperature at which the ESR spectrometer used in the experiment operates. For **(1)**, the line width of the signals shows a slow decrease with decreasing temperature from room temperature to approximately 130 K (see Figs. 5a and 6a). At smaller temperatures, the line width increases vigorously with decreasing temperature. For **(2)**, the line width increases continuously from room temperature to 4.2 K (see Figs. 5b and 6b). These results, due to a strong spin correlation, are in good agreement with those

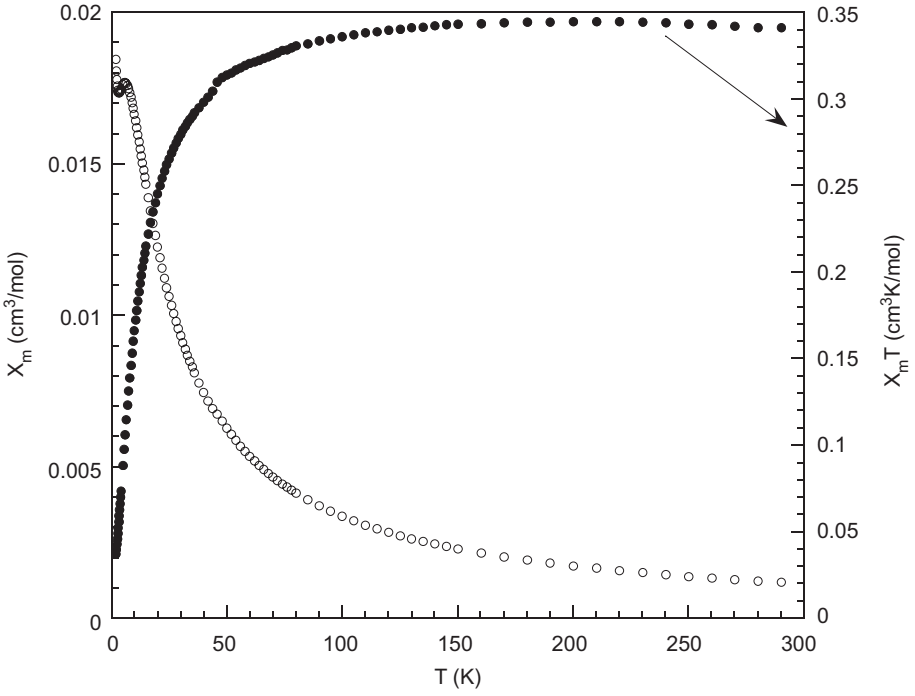

Fig. 7. Thermal evolution of the χ_m and $\chi_m T$ curves of **(1)**.

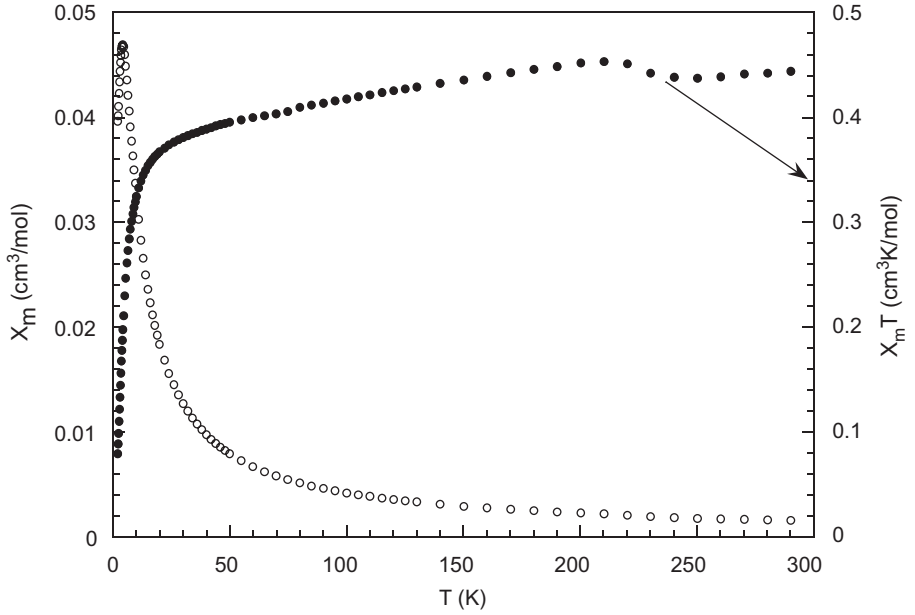

Fig. 8. Thermal evolution of the χ_m and $\chi_m T$ curves of **(2)**.

observed for other magnetic systems, in which the line width also increases drastically when the temperature approximates to the critical one [26].

3.4.2. Magnetic measurements

Magnetic measurements were performed on powdered samples from room temperature to 2.0 K. Plots of the thermal evolution of the χ_m and $\chi_m T$ curves are shown in Figs. 7 and 8, respectively.

The molar magnetic susceptibility increases with decreasing temperature and shows a maximum at, approximately, 6.0 and 4.2 K for compounds **(1)** and **(2),** respectively. For compound **(1)** the χ_m vs. T curve slightly increases from 3.4 to 2 K, probably due to a paramagnetic impurity (see Fig. 4). The thermal evolution of χ_m follows the Curie–Weiss law at temperatures higher than 50 K for compound **(1)**. The calculated Curie and Curie–Weiss constants are $C_m = 0.349\,cm^3\,K\,mol^{-1}$ and $\theta = -4.4$ K. In both phases, the $\chi_m T$ vs. T curve decreases continuously form room temperature to 2.0 K, indicating the existence of antiferromagnetic interactions. However, in phase **(2)** an additional magnetic signal, probably due to an antiferromagnetic impurity with a high temperature for the magnetic coupling, 250–200 K range, is observed in the $\chi_m T$ vs. T curve. The presence of this impurity is supported by the high value of the $\chi_m T$ product, approximately, $0.425\,cm^3\,K\,mol^{-1}$, at 300 K, being the theoretical value for one $(VO)^{2+}$ cation of $0.360\,cm^3\,K\,mol^{-1}$. At low temperature only a continuous decrease in the $\chi_m T$ vs. T curve, due to the antiferromagnetic contributions of both the compound **(2)** and the small portion of the magnetic impurity, is observed; whereas the thermal evolution of the χ_m vs. T curve shows the characteristic features of an antiferromagnetic behavior. This impurity was not observed in the ESR measurements (see Fig. 5b), performed from room temperature to 4.2 K, which show clear isotropic signals characteristic of a unique vanadyl compound with only a paramagnetic center. This impurity was also not detected in the X-ray powder diffraction study, because the patterns only show the characteristic peaks of the phase **(2)**. These facts allow to assign this magnetic signal to an unknown amorphous phase, present in a small proportion together with the piperazinium compound.

Table 6
Bond distances (Å) and angles (°) for the exchange pathways in $R_{0.5}[(VO)(HAsO_4)F]$, with R = ethylenediammonium and piperazinium

Super-exchange-distances (Å)						
Compound **(1)**				Compound **(2)**		
V–F	V–F			V–F		V–F
2.193(1)	1.967(3)			1.959(1)		2.204(1)
Super-exchange: angles (°)						
Compound **(1)**						Compound **(2)**
V–F–V						V–F–V
106.53(2)						106.17(7)
Super-super-exchange: distances (Å)						
Inter-dimers	V–O(3)	O(3)–As	As–O(2)	As–O(1)	O(1)–V	O(2)–V
Compound **(1)**	1.963(3)	1.684(3)	1.669(1)	1.666(1)	2.011(2)	1.990(2)
Compound **(2)**	1.972(2)	1.648(2)	1.692(2)	1.663(2)	2.020(2)	2.021(1)
Intra-dimers	V–O(1)	O(1)–As	As–O(2)	O(2)–V		
Compound **(1)**	2.011(1)	1.616(1)	1.669(2)	1.991(3)		
Compound **(2)**	2.020(2)	1.663(2)	1.691(2)	2.021(2)		
Super-super-exchange: angles (°)						
Inter-dimers	V–O(3)–As	As–O(2)–V	As–O(1)–V	O(3)–As–O(2)		O(3)–As–O(1)
Compound **(1)**	136.694(1)	126.560(2)	120.827(3)	108.79(1)		113.30(1)
Compound **(2)**	137.45(13)	118.97(10)	121.28(10)	109.18(10)		112.76(10)
Intra-dimers	V–O(1)–As	As–O(2)–V	O(1)–As–O(2)			
Compound **(1)**	120.827(1)	126.560(2)	116.61(1)			
Compound **(2)**	121.28(10)	118.97(10)	114.43(10)			

Taking into account the layered crystal structure of these phases, four exchange magnetic pathways between the vanadyl polyhedra can be distinguished. One of them is a super-exchange pathway, and the other three are super-super-exchange pathways, inter- and intra-dimers. The super-exchange pathway takes place through the fluorine atoms with a mean V–F–V angle of 106.3°. The two inter-super-super-exchange pathways and the intra-super-super-exchange pathway involve the V–O(3)–As–O(2,1)–V and V–O(1)–As–O(2)–V angles, with a mean value of 120(9)° and 120(8)°, respectively. The value of these bond angles favors the antiferromagnetic interactions, in good agreement with that observed in the magnetic susceptibility measurements [27]. The bond distances and angles for these exchange pathways are given in Table 6.

4. Concluding remarks

Two new fluoro-vanadyl-hydrogenarsenate compounds, organically templated with ethylenediamine and piperazine, have been synthesized by using mild hydrothermal techniques. The crystal structure of both phases consists of a two-dimensional network constructed from SBU-4 units, which are formed by edge-shared vanadium(IV) octahedra, which are connected to two arsenate tetrahedra by the vertices. This structural unit forms layers along the [1 0 0] direction. The ethylenediammonium and piperazinium cations are located in the interlayer space. The limit of thermal stability is 320 and 340 °C, for the ethylenediamine and piperazine phases, respectively. The diffuse reflectance spectra are characteristic of vanadium(IV), as vanadyl cations, in slightly distorted octahedral environments. The ESR spectra are isotropic for both phases, which exhibit antiferromagnetic exchange couplings.

Acknowledgments

This work has been financially supported by the ''Ministerio de Educación y Ciencia'' (MAT2007-60400) and the ''Gobierno Vasco'' (IT-177-07 and IT-312-07). The authors thank the technicians of SGIker, Drs. I. Orue, F.J. Sangüesa and A. Larrañaga, financed by the National Program for the Promotion of Human Resources within the National Plan of Scientific Research, Development and Innovation, ''Ministerio de Ciencia y Tecnología'' and ''Fondo Social Europeo'' (FSE), for the magnetic measurements and the X-ray diffraction measurement respectively. T. Berrocal wishes to thank the ''Departamento de Investigación y Ciencia del Gobierno Vasco/Eusko Jaurlaritza'' for funding.

References

[1] A.K. Cheetham, G. Férey, T. Loiseau, Angew. Chem. Int. Ed. 38 (1999) 3268.
[2] P.J. Hagrman, D. Hargman, J. Zubieta, Angew. Chem. Int. Ed. 38 (1999) 2638.
[3] G. Férey, Chem. Mater. 13 (2001) 3084.
[4] (a) B. Bazan, J.L. Mesa, J.L. Pizarro, L. Lezama, M.I. Arriortua, T. Rojo, Inorg. Chem. 39 (2000) 6056;
(b) B. Bazan, J.L. Mesa, J.L. Pizarro, A. Goñi, L. Lezama, M.I. Arriortua, T. Rojo, Inorg. Chem. 40 (2001) 5691;
(c) B. Bazan, J.L. Mesa, J.L. Pizarro, M.I. Arriortua, T. Rojo, Mater. Res. Bull. 38 (2003) 3820;
(d) B. Bazan, J.L. Mesa, J.L. Pizarro, L. Lezama, J.S. Garitaonandia, M.I. Arriortua, T. Rojo, Solid State Sci. 5 (2003) 1291;
(e) B. Bazan, J.L. Mesa, J.L. Pizarro, A. Peña, M.I. Arriortua, T. Rojo, Z. Anorg. Allg. Chem. 631 (2006) 2026;
(f) B. Bazan, J.L. Mesa, J.L. Pizarro, L. Lezama, A. Peña, M.I. Arriortua, T. Rojo, J. Solid State Chem. 179 (2006) 1485;
(g) S. Chakrabarti, S.K. Pati, M.A. Green, S. Natarajan, Eur. J. Inorg. Chem. (2004) 3846;
(h) S. Ekambaran, S.C. Sevoc, Inorg. Chem. 39 (2000) 2405;
(i) Y.-C. Liao, S.-H. Luo, S.L. Wang, H.-K. Kao, K.-H. Lii, J. Solid State Chem. 155 (2000) 37;
(j) S. Chakrabarti, M.A. Green, S. Natarajan, Solid State Sci. 4 (2002) 405.
[5] S. Boudin, A. Guesdon, A. Leclaire, M. Borel, Int. J. Inorg. Mater. 2 (2000) 561.
[6] G.W. Coulston, S.R. Bare, H. Kung, K. Birkeland, G.K. Bethke, R. Harlow, N. Herron, P.L. Lee, Science 275 (1997) 191.
[7] J.W. Johnson, A.J. Jacobson, W.M. Butler, S.E. Rosenthal, J.F. Brody, J.T. Lewandowski, J. Am. Chem. Soc. 111 (1989) 381.
[8] R.C. Haushalter, Z. Wang, L.M. Meyer, S.S. Dhingra, M.E. Thompson, J. Zubieta, Chem. Mater 9 (1994) 1463.
[9] A. -H. Liu, S. -L. Wang, Inorg. Chem. 37 (1998) 3415.
[10] Y. Lu, R.C. Haushalter, J. Zubieta, Inorg. Chim. Acta 268 (1998) 257.
[11] V. Soghomonian, R.C. Haushalter, Q. Chen, J. Zubieta, Inorg. Chem. 33 (1994) 1700.
[12] Y.-C. Yang, L.-I. Hung, S.-L. Wang, Chem. Mater. 17 (2005) 2833.
[13] J. Do, R.P. Bontchev, A.J. Jacobson, J. Solid State Chem. 154 (2000) 514.
[14] M. Asnani, S. Sharma, S.E. Lofland, K.V. Ramanujachary, P.A. Buffat, A. Ramanan, Eur. J. Inorg. Chem. (2005) 401.
[15] J.L. Guth, H. Kessler, R. Wey, Stud. Surf. Catal. 28 (1986) 121.
[16] CRYSALIS, version 171.32.5, Oxford Diffraction Ltd., Oxford, 2007.
[17] STOE X-Area, version 1.39, STOE & Cie GmbH, 2006.
[18] G.M. Sheldrick, SHELXS97. Program for the Solution of Crystal Structures, University of Göttingen, Göttingen, Germany, 1997.
[19] G.M. Sheldrick, SHELXL97. Program for the Solution of Crystal Structures, University of Göttingen, Göttingen, Germany, 1997.
[20] International Tables for X-ray Crystallography, vol. IV, Kynoch Press, Birmingham, UK, p. 99.
[21] E. Dowty, ATOMS, A Computer Program for Displaying Atomic Structures, Shape Software, 521 Hidden Valley Road, Kingsport, TN, 1993.
[22] S. Alvarez, D. Avnir, M. Lunell, M. Pinsky, New J. Chem. 26 (2002) 996.
[23] Powder Diffraction File—Inorganic and Organic, File nos. (a) 01-071-2248 and (b) 01-071-0563.
[24] A.B.P. Lever, Inorganic Electronic Spectrosocopy, Elsevier, Amsterdam, 1984.
[25] A. Bencini, D. Gatteschi, EPR of Exchange Coupled Systems, Springer, Berlin, Heidelberg, 1990.
[26] (a) H.W. Wijn, L.R. Walker, J.L. Daris, H. Guggenheim, J. Solid State Commun. 11 (1972) 803;
(b) P.M. Richards, M.B. Salamon, Phys. Rev. B 9 (1974) 32;
(c) A. Escuer, R. Vicente, M.A.S. Goher, F. Mautner, Inorg. Chem. 34 (1995) 5707;
(d) T.T.P. Cheung, Z.G. Soos, R.E. Dietz, F.R. Merrit, Phys. Rev. B 17 (1978) 1266.
[27] J.B. Goodenough, Magnetism and the Chemical Bond, Interscience, New York, 1963.